

A molecular dynamics simulation investigation of the relative stability of the cyclic peptide octreotide and its deprotonated and its (CF₃)-Trp substituted analogs in different solvents

Lorna J. Smith^a, Georgia Rought Whitta^a, Jožica Dolenc^{b,c}, Dongqi Wang^{b,d}, and Wilfred F. van Gunsteren^{b*}

^a Department of Chemistry, University of Oxford, Inorganic Chemistry Laboratory, South Parks Road, Oxford OX1 3QR, United Kingdom

^b Laboratory of Physical Chemistry, Swiss Federal Institute of Technology, ETH, CH-8093 Zurich, Switzerland

^c Current address: Chemistry | Biology | Pharmacy Information Center, ETH, CH-8093 Zurich, Switzerland

^d Current address: Institute of High Energy Physics, Chinese Academy of Sciences, P.O. Box 918, 100049, Beijing, China

* Corresponding author: Professor W. F. van Gunsteren, Laboratory of Physical Chemistry, Swiss Federal Institute of Technology, ETH, CH-8093 Zurich, Switzerland. Email: wfvgn@ethz.ch

Date: 27 July 2016

For: Special Issue Bill Jorgensen, Bioorganic and Medicinal Chemistry (deadline 1/6/2016)

Keywords: octreotide, peptide, molecular dynamics simulation, GROMOS, NMR.

Abbreviations used: CD, circular dichroism; DMSO, dimethyl sulfoxide; LE-TAR, local-elevation time-averaging; MeOH, methanol; MD, molecular dynamics; NMR, nuclear magnetic resonance; NOE, nuclear Overhauser effect; RMSD, root-mean-square difference; RMSF, root-mean-square fluctuation; SPC, simple point charge.

Abstract

The cyclic octa-peptide octreotide and its derivatives are used as diagnostics and therapeutics in relation to particular types of cancers. This led to investigations of their conformational properties using spectroscopic, NMR and CD, methods. A CF₃-substituted derivative, that was designed to stabilize the dominant octreotide conformer responsible for receptor binding, turned out to have a lower affinity. The obtained spectroscopic data were interpreted as to show an increased flexibility of the CF₃ derivative compared to the unsubstituted octreotide, which could then explain the lower affinity.

In this article, we use MD simulation without and with time-averaged NOE distance and time-averaged local-elevation ³J-coupling restraining representing experimental NMR data to determine the conformational properties of the different peptides in the different solvents for which experimental data are available, that are compatible with the NOE atom-atom distance bounds and the ³J_{HNH α} -couplings as derived from the NMR measurements. The conformational ensembles show that the CF₃ substitution in combination with the change of solvent from water to methanol leads to a decrease in flexibility and a shift in the populations of the dominant conformers that are compatible with the experimental data.

1. Introduction

Somatostatin is a cyclic tetradecapeptide which inhibits the release of various hormones including growth hormone, glucagon, insulin and gastrin^{1,2}. Its medicinal application is, however, limited by its plasma half-life shorter than a few minutes³. This induced a search for somatostatin analogs with increased metabolic stability. The cyclic disulfide-bridged octapeptide octreotide⁴ D-Phe¹-Cys²-Phe³-D-Trp⁴-Lys⁵-Thr⁶-Cys⁷-Thr⁸-ol, also known as SMS201-995 or sandostatin, turned out to be a potent inhibitor of growth hormone release⁴ and is used in various medicinal applications (endocrine and malignant disorders) and its derivatives are used as diagnostic⁵ and therapeutic⁶ agents for the detection of and combat against particular types of cancers that are characterized by overexpression, as compared to normal cells, of the somatostatin GCPR of the *hstt*₂ type on the surface of their cells. When binding to the receptors *hstt*₁₋₅, somatostatin, octreotide and analogues are thought to put their Trp⁴-Lys⁵ side chains into receptor pockets⁷. Unfortunately, the sites and structures of these pockets are as yet unknown. Structural investigations using NMR spectroscopy^{8, 9} and X-ray diffraction¹⁰ have shown that octreotide in DMSO solutions adopts a predominant anti-parallel β -sheet conformation characterized by a type II' β -like turn spanning residues D-Trp⁴ and Lys⁵. Similar conformers were found in water/MeOH mixtures⁹ and in one molecule (Model I) of the three molecules in the asymmetric unit of the octreotide crystal¹⁰. The other two molecules (Models II and III) in the asymmetric unit are in a different conformation with the C-terminal part in a helical form (Figure 1).

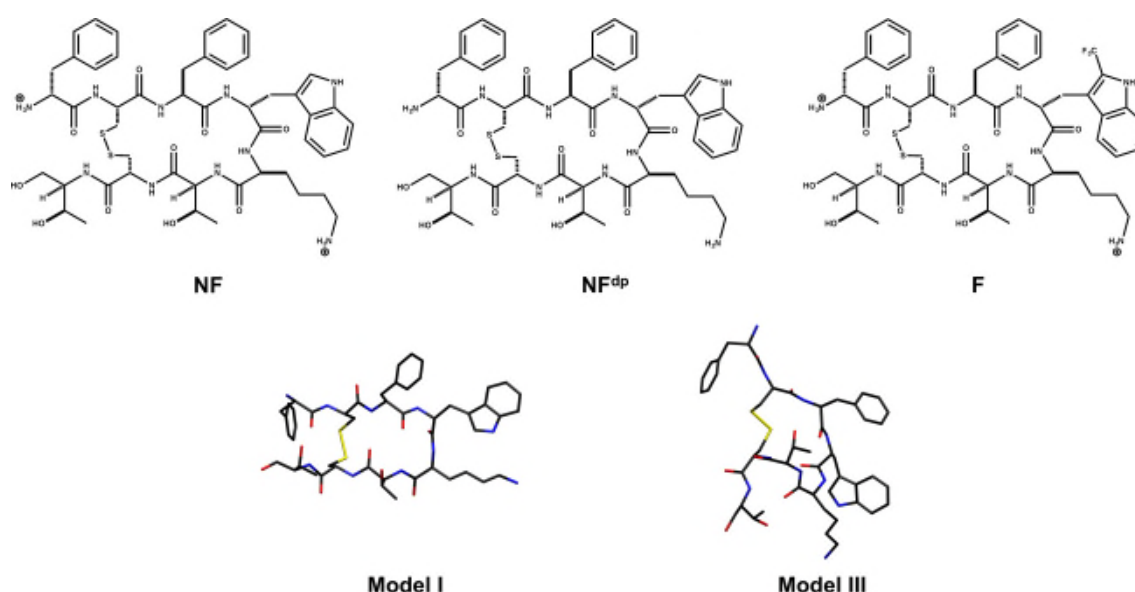


Figure 1. Topologies of the octreotide **1**¹¹ or *NF* (upper left), its deprotonated form *NFdp* (upper middle) and its derivative **3**¹¹ or *F* in which the HD1 atom of D-Trp⁴ is substituted

by a CF₃ group (upper right). Crystal structures Model I and Model III of octreotide *NF* as derived from X-ray diffraction data¹⁰ that served as initial structures for the MD simulations. Oxygens in red, nitrogens in blue, sulfurs in yellow and carbons in black.

The anti-parallel β -sheet conformation can, however, not explain some of the NMR data obtained in DMSO solution¹². Discrepancies were found between some NOE bounds and $^3J_{\text{HNH}\alpha}$ -couplings (Tables 1 and 2) and could be explained¹² by assuming an equilibrium between the conformations Model I and Model III observed in the octreotide crystal. This led to efforts to stabilize particular conformations of octreotide by substitution of its side chains. For example, Seebach et al.¹¹ synthesized four derivatives of octreotide **1** (Figure 1, indicated as *NF*) and experimentally characterized their properties using spectroscopic, NMR and CD, methods. Although it was expected that the substitution of a CF₃ group at carbon C(2) (or CD1) of the Trp 1*H*-indole ring, see octreotide **3** in Figure 1 (indicated as *F*), would reduce the flexibility of the backbone of the cyclic peptide, the NMR¹¹ and CD¹³ spectra were interpreted as to suggest an increased flexibility of the octreotide skeleton by this substitution, which would in turn lead to a lower affinity of binding. Indeed, the affinity of the octreotide *F* to its *hsst*₂-receptor was with a K_d value of 15.5 *nM* lower than that of octreotide *NF*¹¹ with a K_d value of 0.61 *nM*. This counter-intuitive result asked for an investigation of the conformational differences (dominant conformers and flexibility) between octreotides *NF* and *F*, which was carried out using molecular dynamics (MD) simulation methodology.

Table 1. Average $^3J_{\text{HNH}\alpha}$ -coupling values from NMR measurements^{11, 12} calculated from the crystal structures¹⁰ Model I and III and from the 50 ns MD simulations without restraints and with time-averaging NOE distance restraints and local-elevation time-averaging 3J -coupling restraining, each starting from the X-ray structures Model I or Model III.¹⁰ All values in Hz. The value 4.2 Hz for D-Trp⁴ of octreotide *NF* in water was taken from Widmer et al.⁹ replacing the value 3.1 Hz of Seebach et al.¹¹

	Cys ²	Phe ³	D-Trp ⁴	Lys ⁵	Thr ⁶	Cys ⁷	Thr ⁸
Octreotide <i>NF</i> in crystal							
Model I	9.7	7.5	6.6	9.6	9.5	9.5	9.5
Model III	9.3	9.4	3.5	4.7	4.7	5.6	9.3
Octreotide <i>NF</i> in H₂O							
Experiment ¹¹	7.6	7.3	4.2 (3.1)	5.9	7.8	7.7	9.1
Unrestrained Model I	6.9	8.1	6.4	5.6	6.1	7.5	7.8
Unrestrained Model III	6.7	8.0	5.6	5.2	6.1	6.9	7.8
Restrained Model I	7.7	7.3	4.1	5.9	8.0	7.9	9.2
Restrained Model III	7.8	7.3	4.2	6.0	7.9	7.9	9.2
Octreotide <i>NF^{dp}</i> in DMSO							
Experiment ¹²	-	8.8	4.7	8.8	8.1	8.5	8.8
Unrestrained Model I	-	7.8	5.9	6.8	7.1	7.9	6.9
Unrestrained Model III	-	7.8	4.6	4.5	6.4	5.9	7.4
Restrained Model I	-	8.9	4.7	9.2	8.2	9.1	9.1
Restrained Model III	-	9.1	4.6	9.3	8.6	9.1	9.2
Octreotide <i>F</i> in MeOH							
Experiment ¹¹	8.7	7.4	3.8	8.0	9.1	8.8	9.8
Unrestrained Model I	7.9	7.5	4.9	6.8	7.7	8.2	7.4
Unrestrained Model III	6.9	8.3	4.3	4.7	6.3	6.2	7.5
Restrained Model I	9.1	7.5	3.8	8.2	9.3	9.2	9.4

Restrained Model III	9.2	7.3	3.7	8.4	9.2	9.1	9.4
----------------------	-----	-----	-----	-----	-----	-----	-----

Unfortunately, the NMR experimental data,¹¹ $^3J_{\text{HNH}\alpha}$ -couplings and NOE signals for pairs of H- atoms, for the octreotides *NF* and *F* were obtained from measurements of these solutes in different solvents, peptide *NF* in water and peptide *F* in methanol. This means that the differences observed for the two octreotides not only depend on the substitution of the D-Trp⁴ HD1-atom by a CF₃ group, but also upon a change of the solvent water to methanol. Thus the effects of these modifications cannot be separated using the available experimental data. A decade before, NMR $^3J_{\text{HNH}\alpha}$ -couplings and NOEs had been reported for octreotide *NF* in deprotonated form, i.e. NH₂-groups at the N-terminus and the Lys⁵ side chain (indicated as *NF^{dp}*), solvated in DMSO.¹² Previously, octreotide *NF* had been studied using X-ray diffraction of crystals and anisotropic single-structure refinement methodology using high resolution (1.04Å) data.¹⁰ The asymmetric unit contained three *NF* molecules, which appeared to adopt different conformations. While all three molecules exhibit a type II' β-turn involving the -D-Trp⁴-Lys⁵- unit, two different backbone conformations, model I versus model II and III, were found, both probably stabilised by intra-molecular and inter-molecular hydrogen bonds¹⁰: Model I contains the hydrogen bonds 3NH-6O and 8NH-1O (β-turn like) and 6NH-3O (helical), while models II and III contain the hydrogen bonds 6NH-3O and 7NH-4O (helical) and 3NH-6OG1 (side chain). Residues Thr⁶ and Cys⁷ show the largest differences in backbone φ- and ψ- angles: (+130°, +155°) and (-129°, +142°) for model I and (-64°, -18°) and (-71°, -22°) for model III respectively.¹⁰ The crystal structures Model I and III did not reproduce the respective $^3J_{\text{HNH}\alpha}$ -couplings and NOEs measured in water, DMSO or methanol (Tables 1 and 2), which can be due to the differences in crystalline versus solution environment or to uncertainty or error in the NMR data.

Table 2. Number of NOE atom-atom distance bound violations violations in the crystal structures¹⁰ Model I and III and in the 50 *ns* MD simulations without restraints and with time-averaging NOE distance restraints and local-elevation time-averaging ³J-coupling restraining, each starting from the X-ray structure Model I or Model III.¹⁰ The NOE bounds are specified in Table 3 and were based on the NMR data.^{11, 12}

	Range of NOE bound violation (nm)				NOE bounds violated
	0.0-0.05	0.05-0.10	0.10-0.15	0.15-0.25	
Octreotide <i>NF</i> in H₂O	18 NOE distance bounds¹¹				
Model I	1	0	3	1	3 HN - 6 HB, 4 HE3- 5 HA, 5 HA - 7 HN, 6 HN - 7 HN, 6 HA- 8 HN
Model III	3	1	2	0	2 HA - 7 HA, 3 HN - 4HN, 3 HN - 7 HA, 4 HE3 - 5 HA, 6 HA - 7 HN, 7 HA - 8 HN
Unrestrained Model I	0	2	0	0	3 HN - 6 HB, 6 HA - 8 HN
Unrestrained Model III	2	1	0	0	2 HA - 7 HA, 4 HE3 - 5 HA, 6 HN - 8 HN
Restrained Model I	1	0	0	0	6 HN - 7 HN
Restrained Model III	0	0	0	0	
Octreotide <i>NF^d</i> in DMSO	8 NOE distance bounds¹²				
Model I	1	1	0	0	6 HN - 7 HN, 7 HN - 8 HN
Model III	0	2	0	0	6 HA - 7 HN, 7 HA - 8 HN
Unrestrained Model I	1	0	0	0	7 HN - 8 HN
Unrestrained Model III	1	1	0	0	6 HA - 7 HN, 7 HN - 8 HN
Restrained Model I	0	0	0	0	
Restrained Model III	1	0	0	0	6 HN - 7 HN
Octreotide <i>F</i> in MeOH	13 NOE distance bounds¹¹				

Model I	0	0	1	1	4 HE3 - 5 HA, 6 HN - 7 HN
Model III	2	0	1	0	4 HE3 - 5 HA, 6 HA - 7 HN, 7 HA - 8 HN
Unrestrained Model I	0	1	0	0	6 HN - 7 HN
Unrestrained Model III	0	0	0	1	4 HE3 - 5 HA
Restrained Model I	1	0	0	0	6 HN - 7 HN
Restrained Model III	0	0	1	0	6 HN - 7 HN

In view of this variety of experimental data we decided to simulate separately the three peptides *NF*, *NF^{dp}* and *F*, each in the solvent, water, DMSO and methanol, for which experimental NMR data were available, using as two different initial structures the crystal structures model I and model III.¹⁰ In none of these six MD simulations using the GROMOS 54A7 force field¹⁴ the respective $^3J_{\text{HNH}\alpha}$ -couplings and NOEs were entirely reproduced, see Tables 1 and 2, although the agreement is better than for the X-ray diffraction derived crystal structures Model I and Model III. This discrepancy between simulation and experiment can be due to deficiencies of the force field used, to insufficient sampling of the conformational space of the solute, to limited accuracy of the relation between the observable quantity such as 3J -coupling or NOE and a molecular conformation that is used to calculate a 3J -coupling or NOE distance for a conformation, or to inaccuracy of the experimentally measured 3J -coupling or NOE intensity itself.¹⁵

Force-field deficiencies can be addressed by applying 3J -coupling¹⁶ and NOE distance¹⁷ restraints in a MD simulation in a time-averaged manner¹⁸, which allows multiple conformations to contribute to the value of the observable quantity. Conformational sampling for the solute can be enhanced by applying local-elevation sampling¹⁹ to torsional angles that correspond to 3J -couplings when measured values of the 3J -couplings are not reproduced during the restraining MD simulation.²⁰ Thus we repeated the six mentioned MD simulations with time-averaging NOE distance restraining and local-elevation time-averaging 3J -coupling restraining based on the respective sets of NOE bounds (Table 3) and $^3J_{\text{HNH}\alpha}$ -couplings (Table 1).

Table 3. NOE atom pairs and distance upper bounds (in *nm*) used in the NOE distance restraining.

	NOE upper distance bound (nm)		
Proton pairs	Water ¹¹	DMSO ¹²	Methanol ¹¹
D-Phe ¹ HA Cys ² HN	0.26	-	0.26
Cys ² HA Phe ³ HN	0.28	0.27	0.31
Cys ² HA Cys ⁷ HA	0.40	-	-
Phe ³ HN D-Trp ⁴ HN	0.43	-	-
Phe ³ HA D-Trp ⁴ HN	0.26	0.24	0.26
Phe ³ HN Thr ⁶ HN		-	0.47
Phe ³ HN Thr ⁶ HB	0.49	-	-
Phe ³ HN Cys ⁷ HA	0.46	-	-
D-Trp ⁴ HA Lys ⁵ HN	0.25	0.25	0.25
D-Trp ⁴ HE3 Lys ⁵ HA	0.49	-	0.47
D-Trp ⁴ HA Thr ⁶ HN	0.46	-	-
Lys ⁵ HN Thr ⁶ HN	0.31	0.31	0.31
Lys ⁵ HA Thr ⁶ HN	0.45	-	0.47
Lys ⁵ HA Cys ⁷ HN	0.49	-	-
Thr ⁶ HN Cys ⁷ HN	0.33	0.39	0.31
Thr ⁶ HA Cys ⁷ HN	0.31	0.26	0.31
Thr ⁶ HB Cys ⁷ HN	0.47	-	0.47
Thr ⁶ HG2 Cys ⁷ HN			0.64
Thr ⁶ HA Ser ⁸ HN	0.47	-	-
Cys ⁷ HN Ser ⁸ HN		0.36	
Cys ⁷ HA Ser ⁸ HN	0.30	0.27	0.31

Using the $^3J_{\text{HNH}\alpha}$ -coupling values of Seebach et al.¹¹ for octreotide *NF* in water, the reported value for D-Trp⁴ of 3.1 Hz was not reached. Using different restraining function parameters this $^3J_{\text{HNH}\alpha}$ -coupling never got lower than 4.0 Hz and the restraining towards a value of 3.1 Hz pushed the ϕ -angle of Thr⁶ from around - 70° to +60°, which is considered to be sterically unsound. Since values of the 3J -couplings are obtained from peak splittings, their uncertainty becomes larger for smaller values.⁸ Thus it comes as no surprise that a value of 4.2 Hz was reported for D-Trp⁴ in another study of octreotide *NF*.⁹ In view of these considerations we replaced the value 3.1 Hz of Seebach et al.¹¹ by the value 4.2 Hz of

Widmer et al.⁹ for the $^3J_{\text{HNH}\alpha}$ -coupling of D-Trp⁴ in the set of restraints (Table 1).

The goal of our simulation study is threefold.

1. Can the GROMOS 54A7 biomolecular force field reproduce the measured $^3J_{\text{HNH}\alpha}$ -couplings and NOE distance bounds for the octreotides *NF*, *NF^{dp}* and *F* in their respective solvents water, DMSO and methanol, without or with restraining to the sets of measured values of these observable or derived quantities?
2. Is there a structural difference between the dominant conformations of the three octreotides when solvated in water, DMSO or methanol, or when in crystalline form?
3. Is there a difference in conformational stability between octreotide *NF* in water and octreotide *F* in methanol, as suggested by the experimental data?

2. Methods

The topologies of the three solute molecules NF , NF^{dp} and F are shown in Figure 1. Molecule NF^{dp} is identical to NF but for its N-terminus and Lys⁵ side chain being deprotonated, i.e. bearing an NH_2^- instead of an NH_3^- group. Molecule F is identical to NF but for its HD1-atom of D-Trp⁴ being replaced by a CF_3^- group. The GROMOS 54A7 force field^{14,21} was used. It includes solvent models for water (SPC)²², DMSO²³ and methanol.²⁴ The force-field parameters for the CF_3 moiety are specified in Figure S1 and Tables S1 to S4 of Supporting Information. They were derived from standard GROMOS fluorine parameters by analogy reasoning. The most important ones are the following. The lengths of the bonds CD1-C and C-F were 0.153 nm and 0.136 nm, respectively. The value of the ideal bond angles CD1-C-F and F-C-F in the bond-angle bending term of the force field were 111.4° and 107.6°, respectively. The partial charges of the CD1, C and F atoms were 0.05e, 0.46e and -0.17e respectively. The $C_{12}^{1/2}$ (repulsive) and $C_6^{1/2}$ (attractive) Lennard-Jones parameters of the C and F atoms were $1.837 \cdot 10^{-3} (kJ \cdot mol^{-1} \cdot nm^{12})^{1/2}$, $0.04838 (kJ \cdot mol^{-1} \cdot nm^6)^{1/2}$ and $1.000 \cdot 10^{-3} (kJ \cdot mol^{-1} \cdot nm^{12})^{1/2}$, $0.03432 (kJ \cdot mol^{-1} \cdot nm^6)^{1/2}$ respectively.

The initial structures for the solutes in the simulations were Model I and Model III from entry 1302469 (YICMUS) in the Cambridge Structural Database.¹⁰ The peptides were solvated in rectangular boxes and minimum image periodic boundary conditions were applied. The minimum solute-box wall distance was set to 1.2 nm, yielding 2880 water molecules, 863 DMSO molecules, or 1320 methanol molecules. For each of the six systems an equilibration scheme comprising five 20 ps simulations of 60 K, 120 K, 180 K, 240 K and 296 K was used at constant volume. During the first 80 ps of this equilibration the solute atoms were harmonically restrained to their positions in the initial structures (Model I or Model III) with force constants of 25000, 2500, 250 and 25 $kJ \cdot mol^{-1} \cdot nm^{-2}$ at temperatures of 60 K, 120 K, 180 K and 240 K, respectively. Following this equilibration, the simulations were run at 296 K and 1 atm pressure for 50 ns, either without any restraining or using time-averaging NOE distance restraints in combination with local-elevation time-averaging (LE-TAR) $^3J_{HNH\alpha}$ -coupling restraining based on the respective sets of measured NOE atom-atom distance bound and $^3J_{HNH\alpha}$ -coupling values given in Table 3 and Table 1, respectively.

The force constant of NOE distance restraining^{18,21} was $K^{dr} = 10^3 kJ \cdot mol^{-1} \cdot nm^{-2}$, the memory relaxation time τ_{dr} was 5 ps and r³-averaging was performed. For $^3J_{HNH\alpha}$ -coupling restraining the Karplus relation with parameters $a = 6.4 \text{ Hz}$, $b = -1.4 \text{ Hz}$, and $c = 1.9 \text{ Hz}$ was used.²⁵ The LE-TAR force constant was $K^r = 5 \cdot 10^{-3} kJ \cdot mol^{-1} \cdot H^{-4}$, the memory relaxation time

τ_{J_r} was 5 *ps* and the bin width of the local-elevation function^{20, 21} for the torsional angles was 10° ($N_{le}=36$). The biquadratic restraining function had a flat bottom of ± 1 *Hz*. For details of these restraining functions we refer to www.gromos.net.

All simulations were performed at a temperature of 296 *K* and a pressure of 1 *atm* using the weak-coupling algorithm,²⁶ with relaxation times of $\tau_T = 0.1$ *ps* and $\tau_p = 0.5$ *ps* and an isothermal compressibility of $4.575 \cdot 10^{-4}$ (*kJ mol⁻¹ nm⁻³*)⁻¹. Solute and solvent were separately coupled to the heat bath. The SHAKE algorithm²⁷ was used to constrain bond lengths of the solutes and the rigid geometry of the solvent molecules, with a relative geometric tolerance of 10^{-4} allowing for an integration time step of 2 *fs*. The center of mass motion of the system was removed every 1000 time steps. Non-bonded interactions were calculated using a triple-range cutoff scheme with cutoff radii of 0.8 *nm* and 1.4 *nm*. Interactions within 0.8 *nm* were evaluated every time step and intermediate interactions were updated every fifth time step. To account for the influence of the dielectric medium outside the 1.4 *nm* cutoff sphere, a reaction-field force²⁸ with a dielectric permittivity $\epsilon_{RF} = 61$ for water, $\epsilon_{RF} = 46$ for DMSO, and $\epsilon_{RF} = 17.7$ for methanol was used. The solute configurations were saved for analysis every 5 *ps*.

The octreotide configurations were analysed in terms of average NOE atom-atom distances, $^3J_{\text{HNH}\alpha}$ -couplings, atom-positional root-mean-square differences (RMSD) between particular structures, atom-positional root-mean-square fluctuations (RMSF), intra-solute hydrogen bonding occurrences, backbone ϕ - and ψ -angle distributions, and conformational clustering.^{21, 29}

The atom-positional RMSD and RMSF were calculated for the backbone N, CA and C atoms of residues 2 to 7, the cyclic part of the octreotides, after superposition of the molecular centres of mass and a rotational least-squares fit of the positions of these atoms.

A hydrogen bond was considered to exist if the H-O distance is smaller than 0.25 *nm* and the N-H-O angle is larger than 135°.

Conformational clustering was performed using the algorithm of Daura et al.²⁹ and the backbone N, CA and C atoms of residues 2 to 7. The RMSD cutoff used to determine the structures belonging to a single cluster was 0.06 *nm*. Trajectory structures lying 5 *ps* apart were used.

3. Results

3.1 Convergence of the simulations

If a simulation has reached equilibrium and has sufficiently sampled the conformational space of a flexible molecule accessible at the given temperature and pressure, the average quantities calculated from the trajectories of such simulations that started with different initial conditions, *i.e.* atomic coordinates and velocities, should be similar. Comparing the results from the unrestrained simulations starting from the initial structures Model I and Model III in Tables 1 and 2, the expected similarity is largely observed. Differences in averaged $^3J_{\text{HNH}\alpha}$ -couplings larger than 1 Hz are found for D-Trp⁴, Lys⁵ and Cys⁷ in DMSO and for Lys⁵, Thr⁶ and Cys⁷ in methanol (Table 1). Only one NOE distance bound violation larger than 0.1 nm is found in the simulation starting from Model III, while none is found when starting from Model I (Table 2). Comparing the NOE distance and $^3J_{\text{HNH}\alpha}$ -coupling restraining simulations starting from Model I and Model III, the convergence is much improved. The largest difference in $^3J_{\text{HNH}\alpha}$ -couplings is 0.2 Hz and only a single NOE bound violation (6HN-7HN) shows a difference.

$^3J_{\text{HNH}\alpha}$ -couplings and a limited set of NOE atom-atom distance bounds are generally not sufficient to characterize a molecular conformation. Applying a geometric conformational clustering algorithm to two equally large sets of molecular configurations will give an indication of the degree of overlap between the two sets or trajectories of configurations. Figure 2 shows the populations of the ten most populated conformational clusters in the twelve simulations separated according to two consecutive time periods (white: 10-30 ns; black: 30-50 ns). These two periods show similar dominant conformations in the two time periods of molecule *NF* in water (upper panels), except for the unrestrained simulation starting from Model I, where cluster 3 is populated before 30 ns and cluster 2 afterwards. Starting from Model I in DMSO (middle panels) the unrestrained simulation shows a similar change of conformation, cluster 2 is dominant before 30 ns, while cluster 1 is dominant after 30 ns. Molecule *F* in methanol (lower panels) shows less dominant clusters, in particular starting from Model III, while starting from Model I different conformations are accessed after 30 ns.

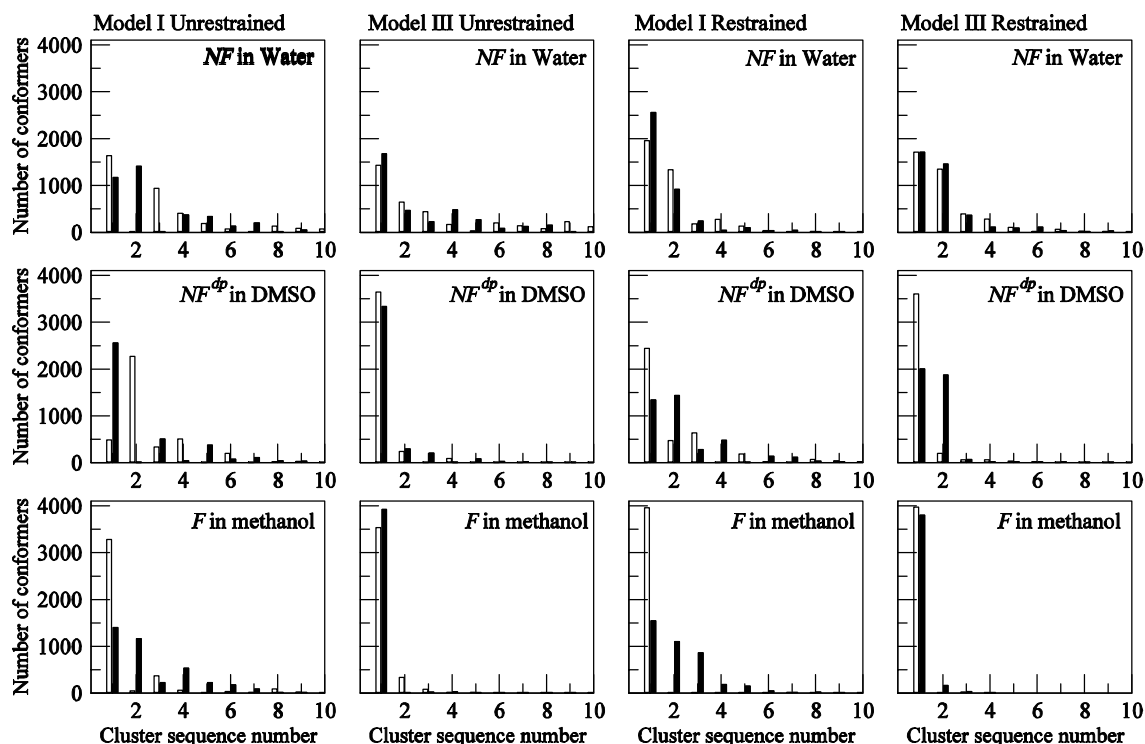
Figure 2

Figure 2. Populations of the ten most populated conformational clusters in the twelve MD simulations separated according to two consecutive time periods (white: 10-30 *ns*; black: 30-50 *ns*) of the three octreotides *NF* in water (upper panels), octreotide *NF^{dp}* in DMSO (middle panels) and octreotide *F* in methanol (lower panels) for the unrestrained (two left columns) and the NOE distance and ³J-coupling restraining (two right columns) 50 *ns* MD simulations starting from the X-ray crystal structures Model I (first and third columns) or Model III (second and fourth columns).

Another way of monitoring sampling and tracking convergence of the simulations is to apply combined conformational clustering to the 30-50 *ns* periods of the two trajectories obtained by starting from the two different initial configurations Model I and Model III (Figure 3). Starting from Model III (black) a broader spread of clusters is populated in water (upper panels) than in starting from Model I (white). In DMSO (middle panels) less convergence is observed, while in methanol (lower panels) starting from Model III leads to fewer clusters than starting from Model I.

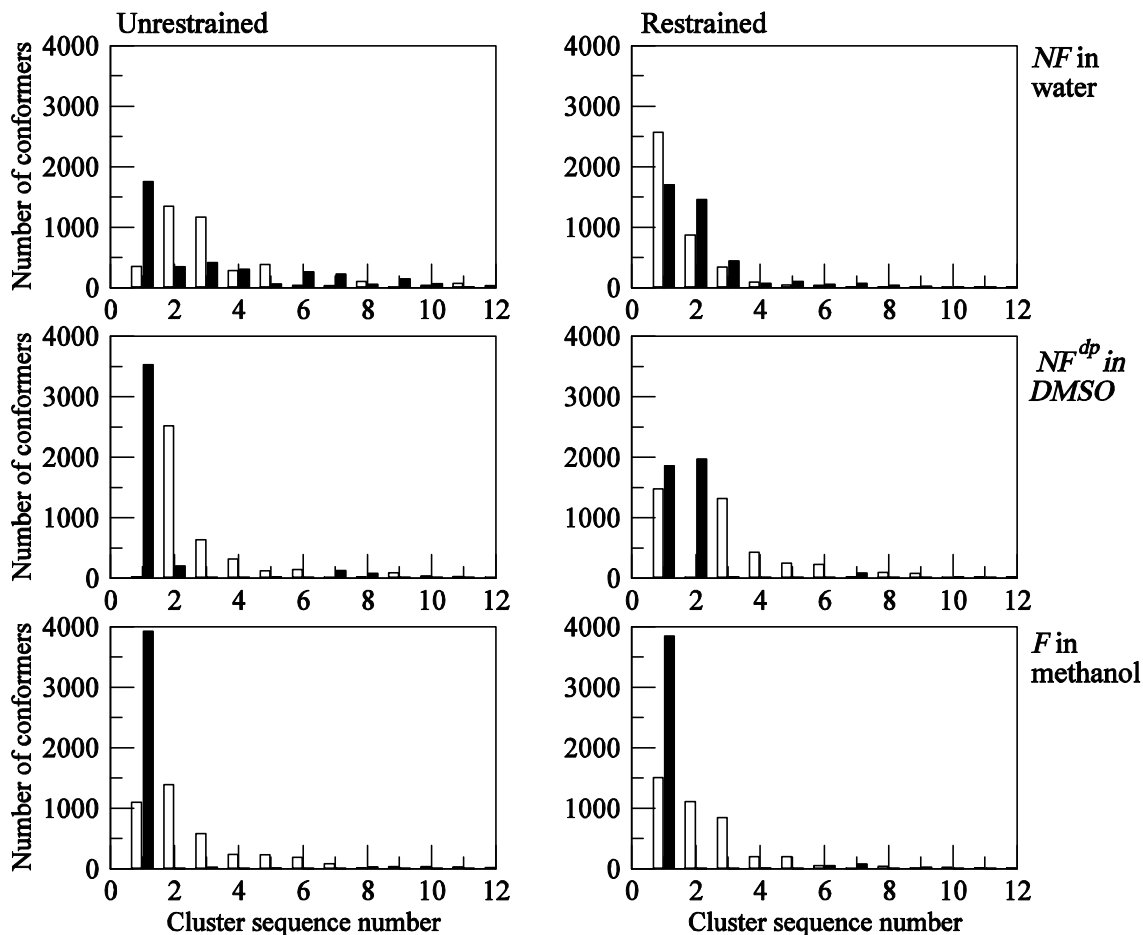
Figure 3

Figure 3. Populations of the twelve most populated conformational clusters in the 30-50 *ns* periods of twelve MD simulations separated according to whether the simulation started from initial structure Model I (white) or from initial structure Model III (black) for the three octreotides *NF* in water (upper panels), octreotide *NF^{dp}* in DMSO (middle panels) and octreotide *F* in methanol (lower panels) and the unrestrained (left column) and the NOE distance and ³J-coupling restraining (right column) 50 *ns* MD simulations starting from the X-ray crystal structures Model I or Model III.

A more detailed picture of the convergence of the backbone conformations can be obtained from Figure 4, which shows the development in time of the backbone atom-positional RMSD between the structures of the twelve 50 *ns* trajectories and the model structures Model I (black) and Model III (grey). For the unrestrained simulations (upper panels) the differences between starting from Model I versus Model III are the largest for DMSO (middle panels) and methanol (right-hand panels). The NOE distance and ³J-coupling simulations starting from Model I and Model III show similar patterns of RMSD values. This matches the observations from Tables 1 and 2. The percentages of hydrogen

bonding reported in Table 4 confirm this picture, less dependence upon the initial structure for octreotide in water than in DMSO or methanol, and a reduction of this dependence by the application of restraints.

Figure 4

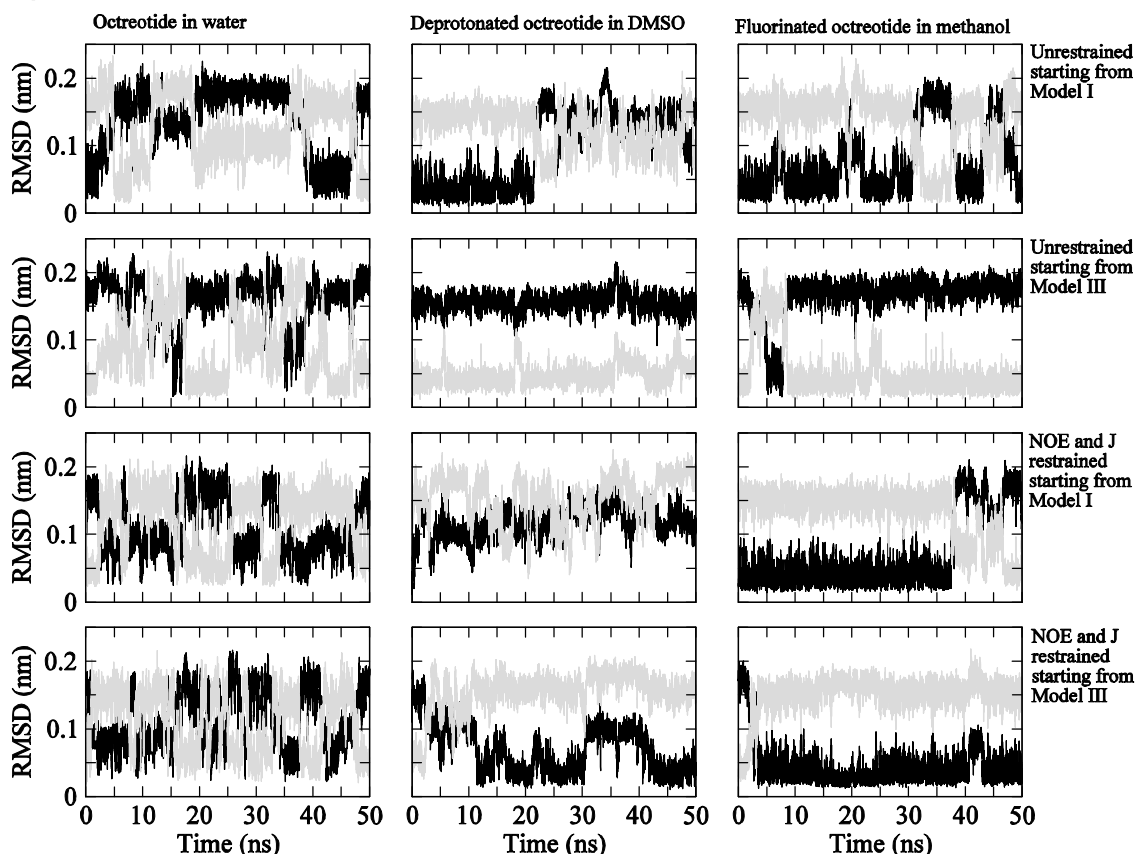


Figure 4. Backbone atom-positional root-mean-square difference (RMSD) (in nm) for residues 2 to 7 between the initial structures Model I (black) or Model III (grey) and the trajectory structures of octreotide *NF* in water (left column), of octreotide *NF^{dp}* in DMSO (middle column) and of octreotide *F* in methanol (right column) from the unrestrained (upper two rows) and from the NOE distance and ³J-coupling restraining (lower two rows) MD simulations starting from the X-ray crystal structure Model I (first and third rows) or Model III (second and fourth rows).

In Figures 5 to 10 the time development of the backbone ϕ - (black) and ψ - (grey) angles for residues 2 to 7 in the twelve simulations are shown. The largest differences between starting from Model 1 versus Model III are observed for residues D-Trp⁴, Thr⁶ and Cys⁷.

Figure 5

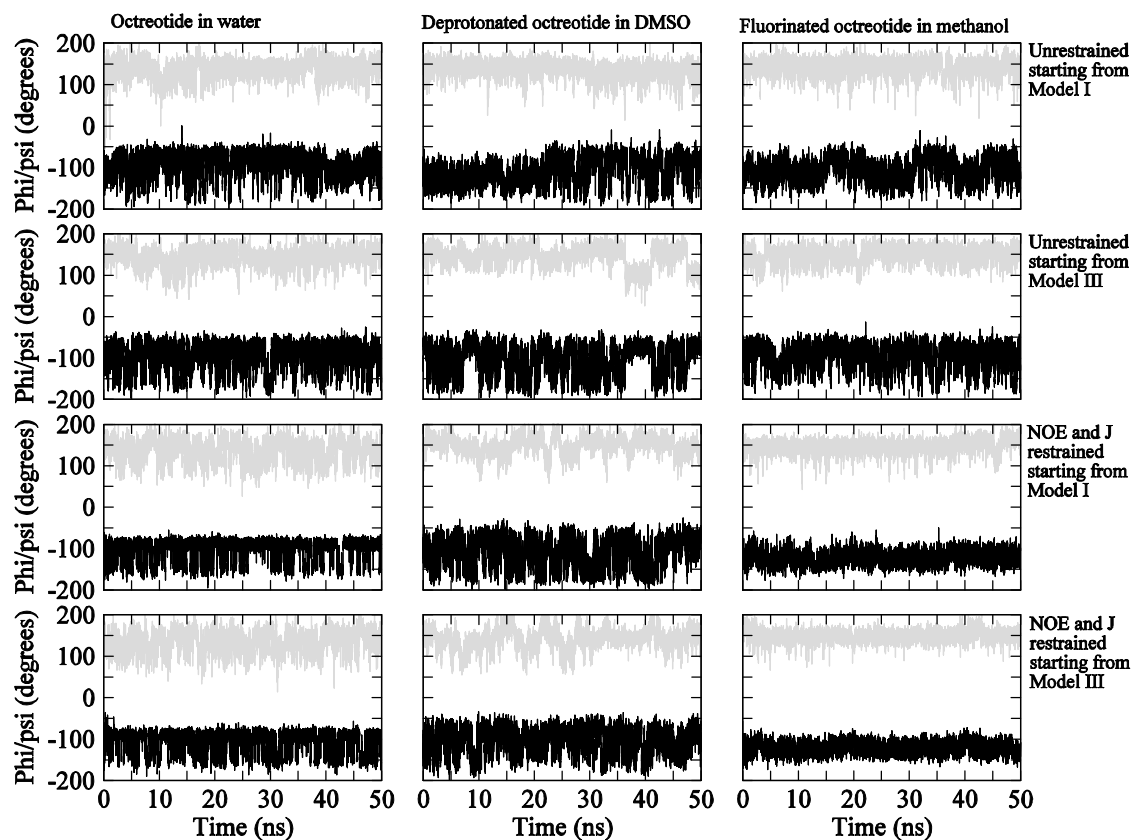


Figure 5. Backbone ϕ - (black) and ψ - (grey) angle values (in degrees) of residue Cys² in the trajectory structures of octreotide *NF* in water (left column), of octreotide *NF^{dp}* in DMSO (middle column) and of octreotide *F* in methanol (right column) from the unrestrained (upper two rows) and from the NOE distance and ³J-coupling restraining (lower two rows) MD simulations starting from the X-ray crystal structure Model I (first and third rows) or Model III (second and fourth rows).

Figure 6

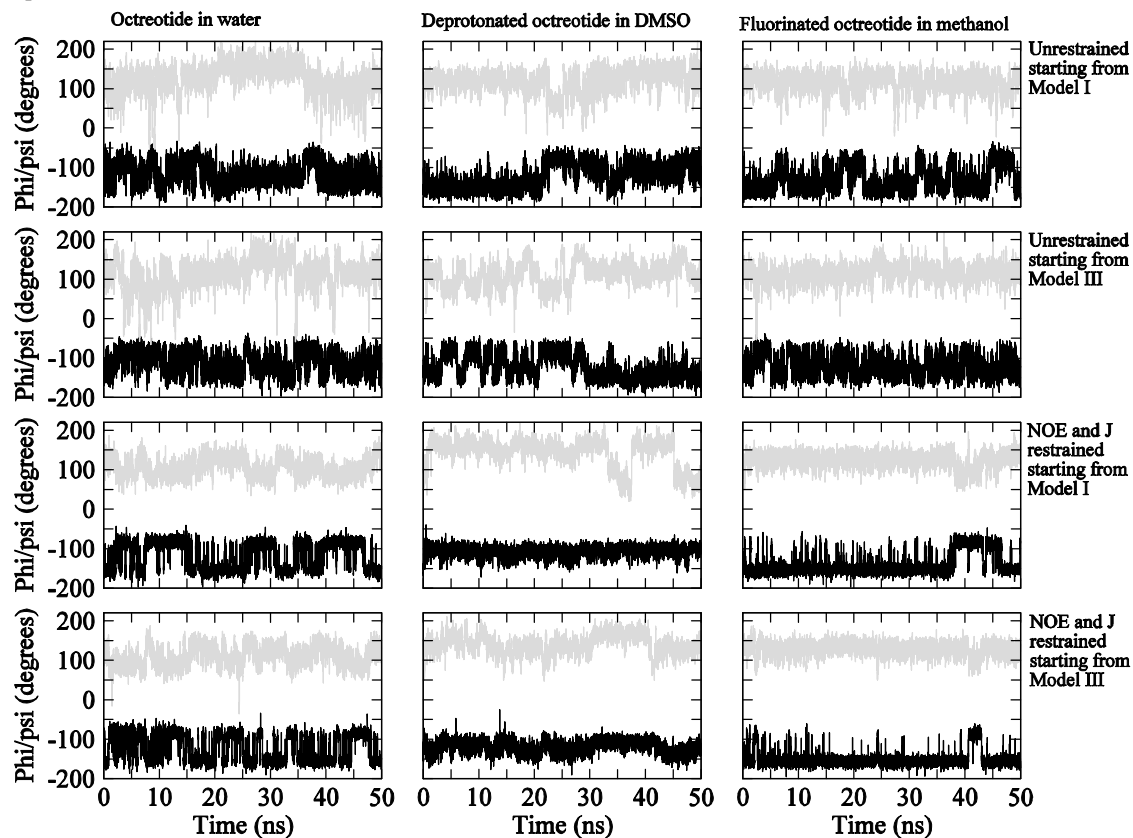


Figure 6. Backbone ϕ - (black) and ψ - (grey) angle values (in degrees) of residue Phe³ in the trajectory structures of octreotide *NF* in water (left column), of octreotide *NF^{dp}* in DMSO (middle column) and of octreotide *F* in methanol (right column) from the unrestrained (upper two rows) and from the NOE distance and ³J-coupling restraining (lower two rows) MD simulations starting from the X-ray crystal structure Model I (first and third rows) or Model III (second and fourth rows).

Figure 7

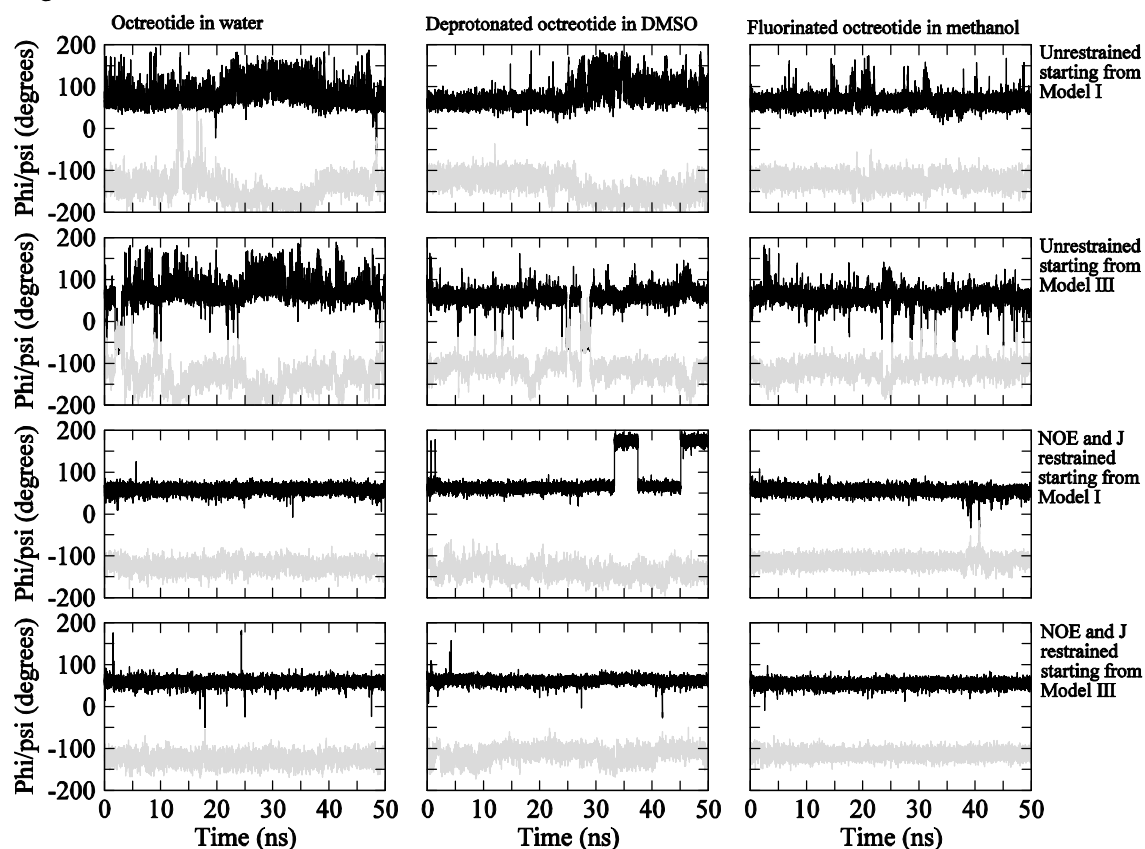


Figure 7. Backbone ϕ - (black) and ψ - (grey) angle values (in degrees) of residue D-Trp⁴ in the trajectory structures of octreotide *NF* in water (left column), of octreotide *NF^{dp}* in DMSO (middle column) and of octreotide *F* in methanol (right column) from the unrestrained (upper two rows) and from the NOE distance and ³J-coupling restraining (lower two rows) MD simulations starting from the X-ray crystal structure Model I (first and third rows) or Model III (second and fourth rows).

Figure 8

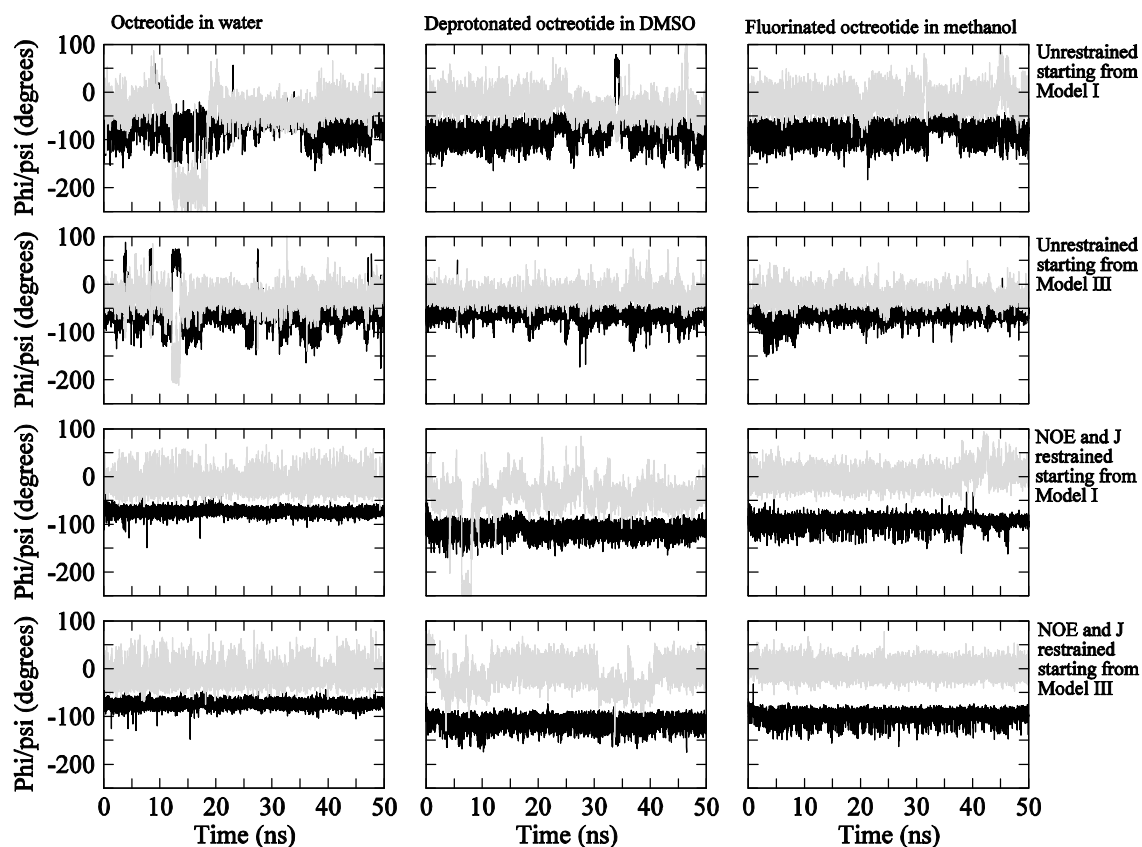


Figure 8. Backbone ϕ - (black) and ψ - (grey) angle values (in degrees) of residue Lys⁵ in the trajectory structures of octreotide *NF* in water (left column), of octreotide *NF^{dp}* in DMSO (middle column) and of octreotide *F* in methanol (right column) from the unrestrained (upper two rows) and from the NOE distance and ³J-coupling restraining (lower two rows) MD simulations starting from the X-ray crystal structure Model I (first and third rows) or Model III (second and fourth rows).

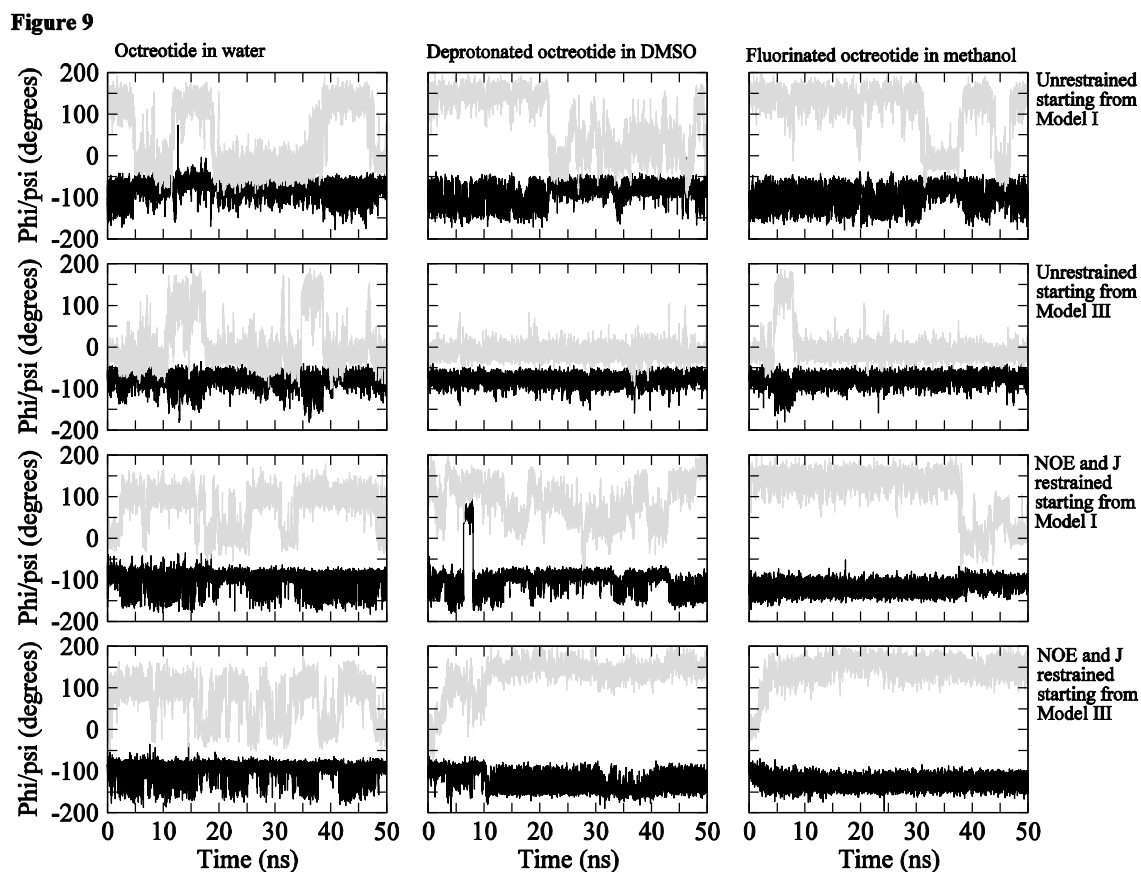


Figure 9. Backbone ϕ - (black) and ψ - (grey) angle values (in degrees) of residue Thr⁶ in the trajectory structures of octreotide *NF* in water (left column), of octreotide *NF^{dp}* in DMSO (middle column) and of octreotide *F* in methanol (right column) from the unrestrained (upper two rows) and from the NOE distance and ³J-coupling restraining (lower two rows) MD simulations starting from the X-ray crystal structure Model I (first and third rows) or Model III (second and fourth rows).

Figure 10

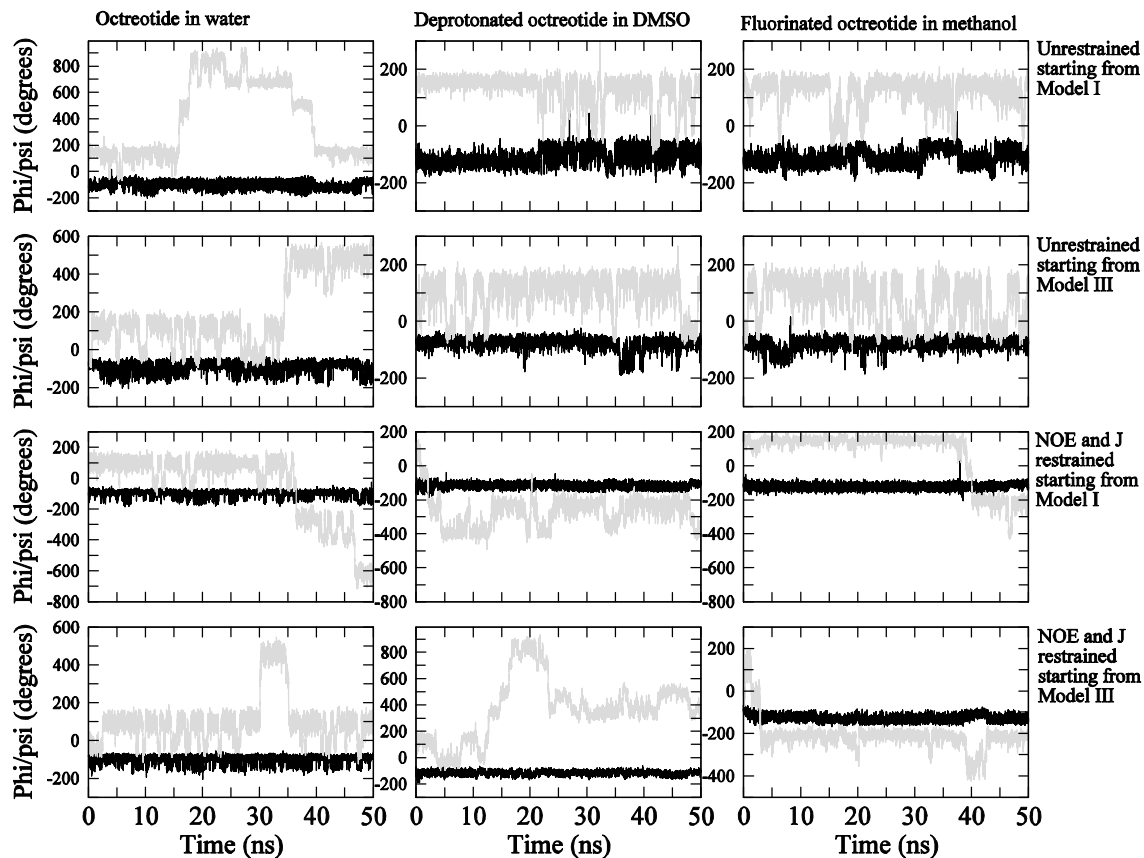


Figure 10. Backbone ϕ - (black) and ψ - (grey) angle values (in degrees) of residue Cys⁷ in the trajectory structures of octreotide *NF* in water (left column), of octreotide *NF^{dp}* in DMSO (middle column) and of octreotide *F* in methanol (right column) from the unrestrained (upper two rows) and from the NOE distance and ³J-coupling restraining (lower two rows) MD simulations starting from the X-ray crystal structure Model I (first and third rows) or Model III (second and fourth rows).

The backbone atom-positional fluctuations (RMSF) show a similar pattern between starting from Model I and Model III (Figure 11, compare black with red and green with blue). Starting from Model III the fluctuations are smaller than starting from Model I in DMSO or in methanol.

Figure 11

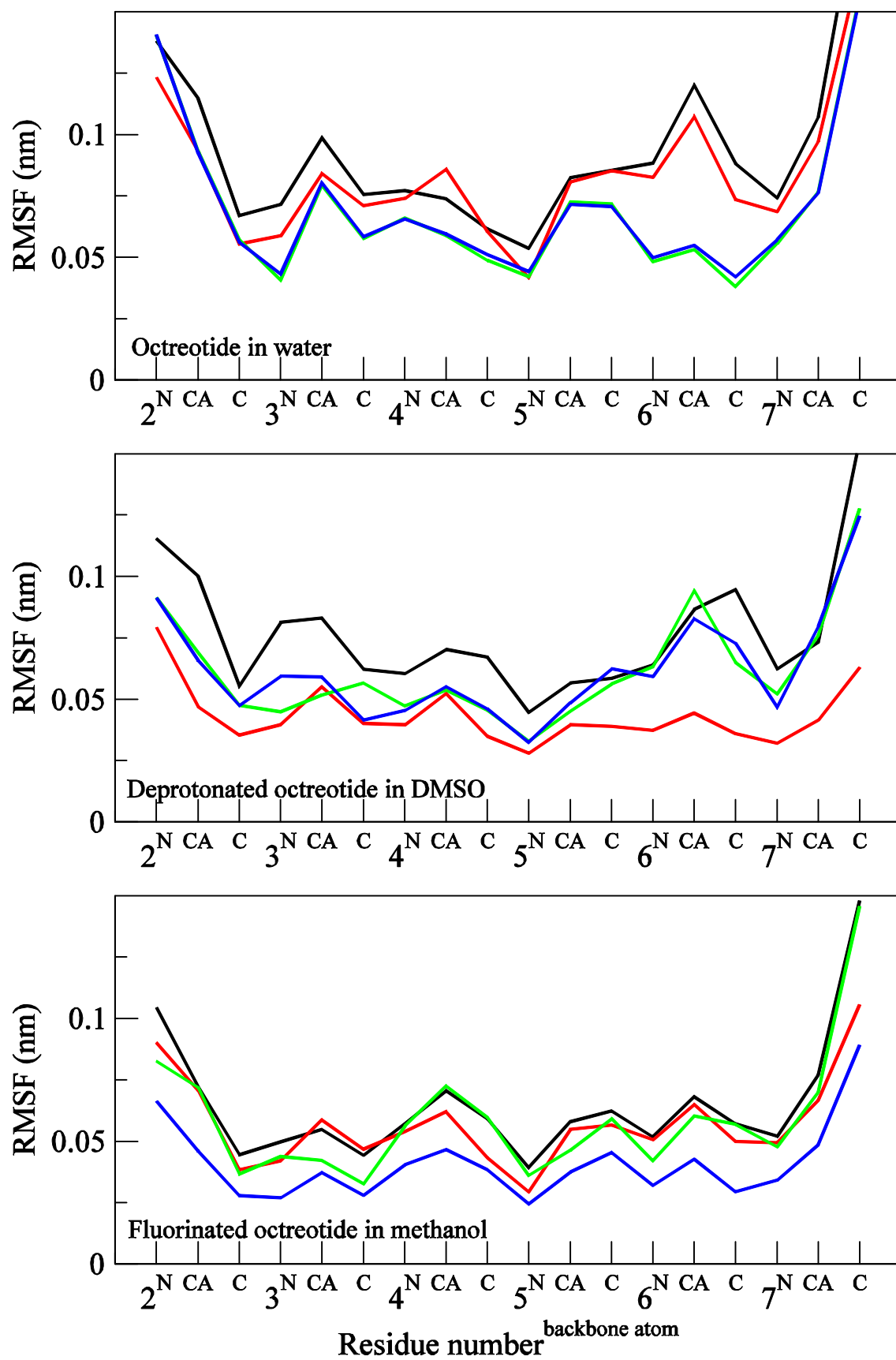


Figure 11. Backbone atom-positional root-mean-square fluctuations (RMSF) (in nm) for residues 2 to 7 in the trajectory structures of octreotide *NF* in water (upper panel), of octreotide *NF^{dp}* in DMSO (middle panel) and of octreotide *F* in methanol (lower panel) from the unrestrained (black and red) and from the NOE distance and ³J-coupling restraining (green and blue) 50 ns MD simulations starting from the X-ray crystal structure Model I (black and green) or Model III (red and blue).

Finally, Figure 12 shows that when starting from Model III in DMSO (red bars) or in methanol (green bars) there is less conformational heterogeneity than when starting from Model I.

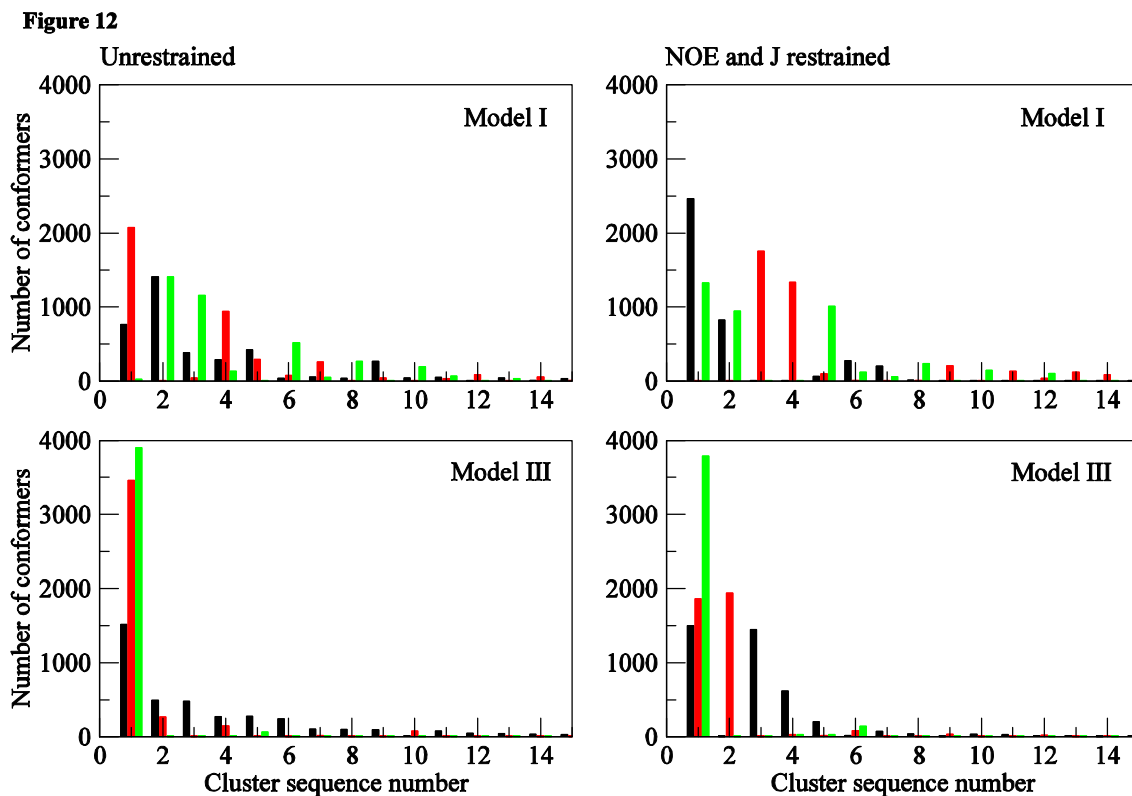


Figure 12. Populations from conformational clustering of the trajectory structures of the three octreotides *NF* in water (black), octreotide *NF^{dp}* in DMSO (red) and octreotide *F* in methanol (green) for the 30 – 50 ns periods for the unrestrained (left panels) and the NOE distance and ³J-coupling restraining (right panels) 50 ns MD simulations starting from the

X-ray crystal structures Model I (upper panels) or Model III (lower panels).

Some simulations were extended to 150 *ns*, but this did not improve the convergence significantly. Apparently, the energetic barriers separating the conformational spaces around the conformations Model I and III require a long time period in order to be surmounted.

3.2 Comparison with experimental data

The unrestrained simulations do not satisfy all NOE distance bounds (Table 2) and do not reproduce all measured $^3J_{\text{HNH}\alpha}$ -couplings (Table 1). Considering the uncertainty of an NOE distance bound inherent to its derivation from an NOE signal intensity, we only consider NOE distance bound violations larger than 0.1 *nm* unsatisfactory. Although $^3J_{\text{HNH}\alpha}$ -couplings can generally be measured accurately, a sizeable uncertainty of 1-2 *Hz* is introduced in calculated $^3J_{\text{HNH}\alpha}$ -couplings due to the approximate nature of the Karplus relation linking a 3J -coupling to a torsional angle.³⁰

The unrestrained simulations show the largest deviations from the measured $^3J_{\text{HNH}\alpha}$ -couplings for residues D-Trp⁴ (1.4 - 2.2 *Hz*), Thr⁶ (1.7 *Hz*) and Thr⁸ (1.3 *Hz*) in water, for residues Lys⁵ (2.0 - 4.3 *Hz*), Thr⁶ (1.0 - 1.7 *Hz*), Cys⁷ (0.6 - 2.6 *Hz*) and Thr⁸ (1.4 - 1.9 *Hz*) in DMSO, and for residues Cys² (0.8 - 1.8 *Hz*), Lys⁵ (1.2 - 3.3 *Hz*), Thr⁶ (1.4 - 2.8 *Hz*), Cys⁷ (0.6 - 2.6 *Hz*) and Thr⁸ (2.3 - 2.4 *Hz*) in methanol. Only for methanol one NOE bound violation (4HE3-5HA) larger than 0.1 *nm* was observed starting from Model III.

These results led us to applying time-averaging NOE distance and local-elevation 3J -coupling restraining in the MD simulations in order to improve the agreement with the experimental data while enhancing the torsional-angle sampling. The measured $^3J_{\text{HNH}\alpha}$ -couplings are reproduced within 0.2 *Hz* for water, 0.6 *Hz* for DMSO, and 0.5 *Hz* for methanol. Only one NOE bound violation (6HN- 7HN) is observed in all three solvents. The NOE distance and 3J -coupling restrained MD trajectories may thus be considered as conformational ensembles resulting from time-averaging multi-structure refinement based on the available experimental data. These ensembles will be used to analyse the conformational properties of the octreotides in the different solvents in the next sections. We note, however, that the change in the conformational ensemble induced by the application of time-averaging restraining is rather small. Figure 13 shows the results from

combined conformational clustering of the 30-50 *ns* periods of the unrestrained and the $^3J_{\text{HNH}\alpha}$ -coupling and NOE distance bound time-averaging restrained trajectories. The application of the 3J -coupling and NOE atom-atom distance restraints did show some changes in the relative populations of the dominant conformational clusters, starting from Model I in water and in DMSO, and in particular starting from Model III in DMSO and methanol. It is noteworthy that the restraining does not limit the conformational variety. Although in water (upper panels) the number of significantly populated clusters is reduced, in DMSO (middle panels) and also starting from Model III in methanol (lower panels) restraining leads to a lower population of the most populated cluster. This indicates that the experimental data are representing more than a single molecular conformation. The atom-positional fluctuations in water are reduced and, as expected, the ϕ/ψ torsional-angle fluctuations are also reduced. In addition, the restraints destabilize the Model III conformation in methanol.

Figure 13

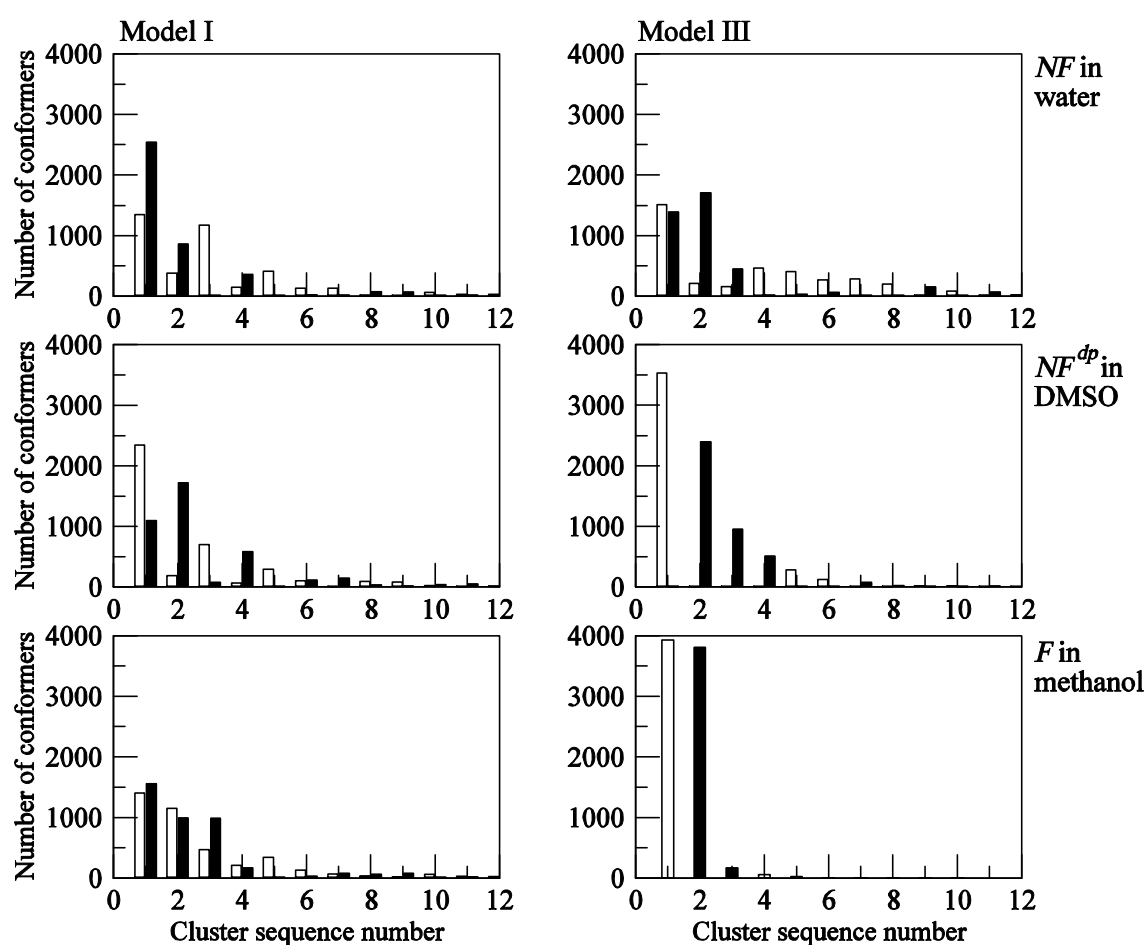


Figure 13. Populations of the twelve most populated conformational clusters in the 30-50 ns periods of twelve 50 ns MD simulations separated according to whether the simulation was unrestrained (white) or used NOE atom-atom distance and ^3J -coupling restraining (black), started from X-ray crystal structures Model I (left column) or Model III (right column) for the three octreotides *NF* in water (upper panels), octreotide *NF^d* in DMSO (middle panels) and octreotide *F* in methanol (lower panels).

3.3 Comparison of the three octreotides in their respective solvents

Figure 4 (lower panels) shows that octreotide *NF* in water switches more rapidly between conformations Model I and Model III than octreotide *NF^d* in DMSO or octreotide *F* in methanol. The ϕ -angles (black) of residues Cys² (Figure 5) and Phe³ (Figure 6) show larger fluctuations in water and DMSO than in methanol. In Lys⁵ (Figure 8) the ϕ -angle adopts larger values in water than in DMSO or methanol. The ψ -angles (grey) of Thr⁶ (Figure 9) and Cys⁷ (Figure 10) show larger variations for all three octreotides in their three solvents.

The backbone atom-positional fluctuations (Figure 11) are largest in water and smallest in methanol, although in methanol only 13 NOE bounds had been derived from NOE signals, whereas in water there were 18 NOE bounds.

The percentages of hydrogen bonding (Table 4) show least hydrogen bonding for *NF^d* in DMSO and most stable hydrogen bonds (6HN-30, 3HN-60, 8HN-10) in methanol which is in line with the small atom-positional fluctuations observed in methanol.

Table 4. Percentage of hydrogen bonds in the 50 ns MD simulations without restraints and with time-averaging NOE distance restraints and local-elevation time-averaging ³J-coupling restraining, each starting from the X-ray structure Model I or Model III.¹⁰ All values in Hz. A hydrogen bond is defined by a maximum H – O distance of 0.25 nm and a minimum N – H – O angle of 135°.

	backbone NH → O										NH→OG1
	helical				β-turn-like		<i>i</i> → <i>i</i> -2				side chain
	6-3	7-4	8-4	8-5	3-6	8-1	4-2	6-4	7-5	8-6	3-6
Octreotide <i>NF</i> in H₂O											
Unrestrained Model I	10	22	17	2	17	15	3	0	6	3	7
Unrestrained Model III	20	41	8	3	4	1	8	1	7	5	20
Restrained Model I	59	14	1	0	38	12	5	4	11	11	17
Restrained Model III	53	16	2	1	36	10	5	5	12	12	16
Octreotide <i>NF_{dp}</i> in DMSO											
Unrestrained Model I	27	12	0	1	41	42	8	1	18	5	0
Unrestrained Model III	55	68	1	3	0	0	14	0	2	13	55
Restrained Model I	3	0	0	0	1	0	7	1	24	6	0
Restrained Model III	55	0	0	0	48	18	1	1	5	3	2
Octreotide <i>F</i> in MeOH											
Unrestrained Model I	49	9	0	0	62	48	6	1	4	6	7
Unrestrained Model III	56	66	4	11	6	5	6	0	3	12	53
Restrained Model I	85	5	1	0	73	68	4	3	3	1	7
Restrained Model III	94	1	0	0	91	76	1	1	0	1	3

Figure 14 shows the results of the pairwise combined conformational clustering of two 3J -coupling and NOE atom-atom distance restrained trajectories (30-50 *ns* periods) taken from the three systems *NF* in water, *NF^{dp}* in DMSO and *F* in methanol. Starting from Model I (left panels) a quite disjoint distribution of cluster populations is observed between DMSO and the other two solvents, although the most populated cluster is the same for methanol and water. Starting from Model III the most populated cluster is the same between methanol and the other two solvents and almost the same between water and DMSO, and in water a wider variety of conformations is observed.

Figure 14

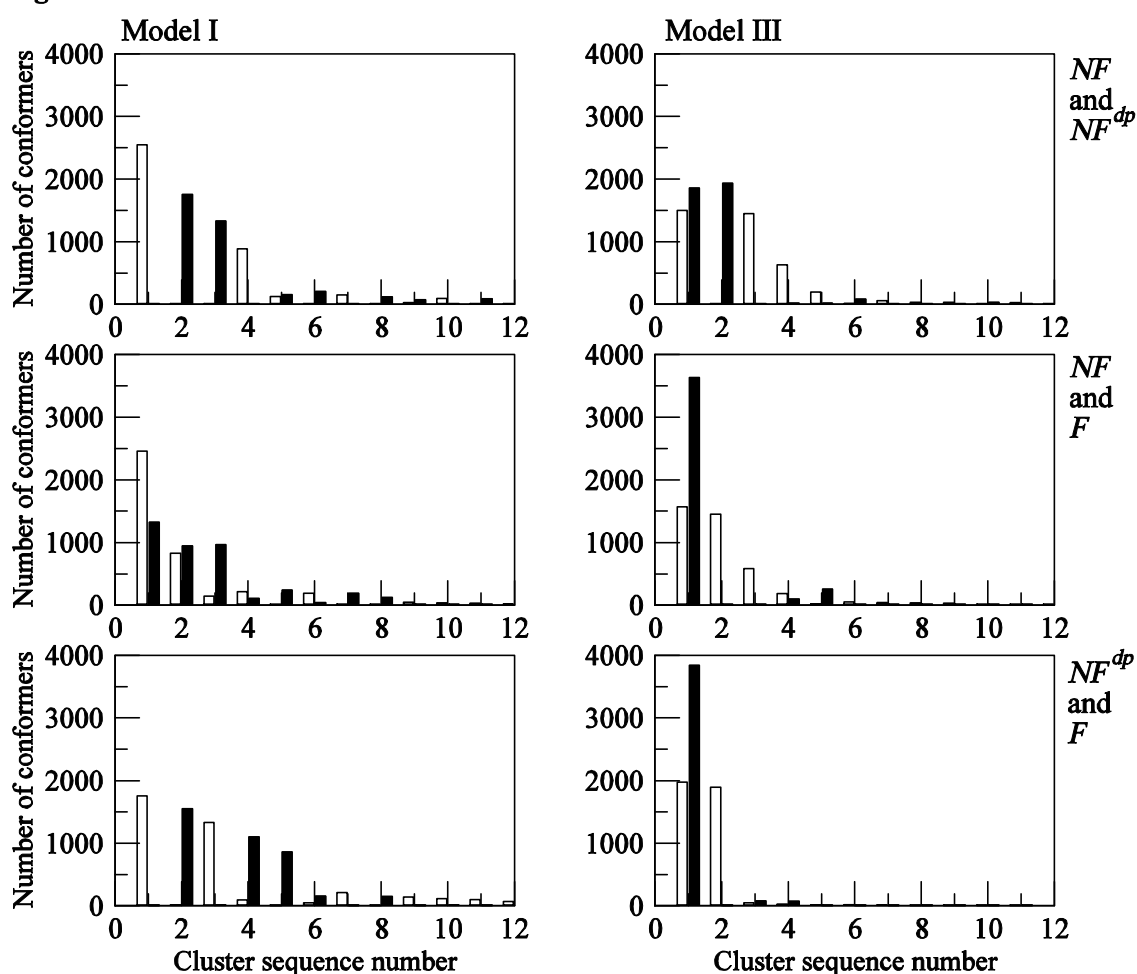


Figure 14. Populations of the twelve most populated conformational clusters in the 30-50 *ns* periods of twelve 50 *ns* MD simulations separated according to whether the system consisted of peptide *NF* in water, peptide *NF^{dp}* in DMSO or peptide *F* in methanol. Upper panels: peptide *NF* in water (white) versus peptide *NF^{dp}* in DMSO (black). Middle panels peptide *NF* in water (white) versus peptide *F* in methanol (black). Lower panels: peptide

NF^{dp} in DMSO (white) versus peptide F in methanol (black). Left column: simulations started from the X-ray crystal structure Model I. Right column: simulations started from the X-ray crystal structure Model III.

The combined conformational clustering of the three trajectories of NF , NF^{dp} and F shows differences between the contributions of the three molecules to the most dominant conformational clusters (Figure 12). In the three simulations (NF : black, NF^{dp} : red, F : green) starting from Model I, only cluster 5 shows relatively equal contributions from all three trajectories (upper right panel). In these simulations the octreotides NF in water (black) and F in methanol (green) adopt conformations different from those of octreotide NF^{dp} in DMSO (red). Starting from Model III the picture is different, partially because the sequence of the in total most populated clusters has changed. Still, the three octreotides in their different solvents adopt various conformations with different weights.

Table 3 shows that for octreotide NF in water there are 6 NOEs between non-sequential residues, whereas for NF^{dp} in DMSO there are none, and for F in methanol there is one such NOE observed (Phe³-Thr⁶). Table 1 shows that the measured values of the $^3J_{\text{HNH}\alpha}$ -couplings increase going from NF in water to NF^{dp} in DMSO except for Thr⁸, and that the same trend is observed going from NF in water to F in methanol, except for D-Trp⁴. These differences push the peptide from being a more equal mixture of β -turn like Model I and helical Model III conformations in water to being more β -turn like in methanol. In water and in methanol the ϕ - and ψ -angles adopt values in ranges around those of Model I and Model III. However, in DMSO, where there are less data and a change in the relative NOE distances involving residues 6 and 7, a third conformation appears which has fewer hydrogen bonds.

3.4 Relative conformational stability of octreotides NF and F

The introduction of a CF_3 group at the CD1 atom of the side chain of D-Trp⁴ was thought to stabilise the conformation of the octreotide. Indeed, the backbone atom-positional fluctuations of octreotide F in methanol are smaller than those of octreotide NF in water (Figure 11). We did not observe any hydrogen bond involving the fluorine atoms that could explain this. This might suggest that the change of solvent from water to methanol has a larger influence on the dominant conformation of the octreotide than the substitution of an H-atom by a CF_3 group in the D-Trp⁴ side chain. This substitution combined with a change of solvent from water to methanol induces a shift in the equilibrium between the different conformations dominating the structural ensemble,

thereby stabilizing a particular conformation. If this conformation is different from the one that most readily binds octreotide to its *hsst*₂-receptor and if this conformational shift is not largely due to the change of solvent from water to methanol, it might explain the lower binding affinity of the CF₃-substituted peptide. Unfortunately, the fact that the three different molecules were experimentally investigated in three different solvents rendered a delineation of the substitution and solvent effects upon the dominant conformation and the flexibility of the molecules impossible.

4. Conclusions

Using twelve 50 ns MD simulations, six without and six with time-averaged NOE distance restraining in combination with time-averaged local-elevation ³J_{HNH α} -coupling restraining, for three systems, octreotide *NF* in water, its deprotonated form *NF^{dp}* in DMSO, and its derivative *F* that has a CF₃ group at the CD1 atom of D-Trp⁴ in methanol, starting from two different X-ray crystal structures, Model I and Model III, the conformational properties of the three peptides in their respective solvents were analyzed, because these were thought to be responsible for the loss of affinity of octreotide for its receptor by the CF₃ substitution.

Since the experimental data were obtained for the three peptides each in a different solvent, the effects of a change in composition of the peptide versus of the solvent could not be delineated based on the experimental data.

The results illustrate that (i) interpreting crystal structures as relevant to interpreting solution (NMR) data is often not warranted, (ii) single-structure refinement based on experimental data of a limited set of values of observables can lead to incorrect interpretation of the latter due to the presence of more than one conformer in solution, and (iii) in such a case time-averaging structure refinement is mandatory and so is the use of enhanced sampling techniques such as local-elevation search to capture the different conformations accessible to a molecule in solution.

Peptide *F* in methanol shows less flexibility than peptide *NF* in water, while the observation that more and longer-range NOE signals could be identified for peptide *NF* in water than for peptide *F* in methanol would have suggested the contrary. The simulations show that a shift in the populations of the dominant conformations of the octreotide upon the CF₃ substitution combined with a change of solvent from water to methanol leads to smaller backbone torsional-angle fluctuations in Phe³ and Thr⁶ for peptide *F* than for

peptide *NF*. If one assumes that the β -turn region of the peptide is responsible for its binding to the receptor, the lower binding affinity of peptide *F* compared to peptide *NF* may be explained by the more rigid fold of peptide *F* observed in the simulations. The less flexible peptide *F* cannot adapt its conformation to the receptor pocket while the more flexible peptide *NF* can adapt itself better to the binding site, because it may change the Phe³ and Thr⁶ backbone angles easier while retaining the D-Trp⁴-Lys⁵ β -turn.

Acknowledgements

The authors gratefully acknowledge the contribution of Alexander L. Kunze who conducted during the fall of 2010 as a student at the ETH a preliminary investigation of the octreotide. LJS and GRW would like to acknowledge the use of the University of Oxford Advanced Research Computing (ARC) facility in carrying out some of this work. <http://dx.doi.org/10.5281/zenodo.22558>.

This article is dedicated to Bill Jorgensen in honour of his many excellent contributions to the field of molecular modeling of medicinal compounds.

References

1. Reichlin, S. *New Engl. J. Med.* **1983**, *309*, 1495-1501.
2. Reichlin, S. *New Engl. J. Med.* **1983**, *309*, 1556-1563.
3. Kaupmann, K.; Bruns, C.; Raulf, F.; Weber, H. P.; Mattes, H.; Lubbert, H. *EMBO J.* **1995**, *14*, 727-735.
4. Bauer, W.; Briner, U.; Doepfner, W.; Haller, R.; Huguenin, R.; Marbach, P.; Petcher, T. J.; Pless, J. *Life Sci.* **1982**, *31*, 1133-1140.
5. Reubi, J. C.; Maecke, H. R. *J. Nucl. Med.* **2008**, *49*, 1735-1738.
6. van der Hoek, J.; Hofland, L. J.; Lamberts, S. W. J. *Curr. Pharm. Des.* **2005**, *11*, 1573-1592.
7. Seebach, D.; Dubost, E.; Mathad, R. I.; Jaun, B.; Limbach, M.; Loweneck, M.; Flogel, O.; Gardiner, J.; Capone, S.; Beck, A. K.; Widmer, H.; Langenegger, D.; Monna, D.; Hoyer, D. *Helv. Chim. Acta* **2008**, *91*, 1736-1786.
8. Wynants, C.; Vanbinst, G.; Loosli, H. R. *Int. J. Pept. Protein Res.* **1985**, *25*, 615-621.
9. Widmer, H.; Widmer, A.; Braun, W. *J. Biomol. NMR* **1993**, *3*, 307-324.
10. Pohl, E.; Heine, A.; Sheldrick, G. M.; Dauter, Z.; Wilson, K. S.; Kallen, J.; Huber, W.; Pfaffli, P. J. *Acta Cryst. D* **1995**, *51*, 48-59.
11. Seebach, D.; Widmer, H.; Capone, S.; Ernst, R.; Bremi, T.; Kieltsch, I.; Togni, A.; Monna, D.; Langenegger, D.; Hoyer, D. *Helv. Chim. Acta* **2009**, *92*, 2577-2586.
12. Melacini, G.; Zhu, Q.; Goodman, M. *Biochemistry* **1997**, *36*, 1233-1241.
13. Capone, S.; Kieltsch, I.; Flogel, O.; Lelais, G.; Togni, A.; Seebach, D. *Helv. Chim. Acta* **2008**, *91*, 2035-2056.
14. Schmid, N.; Eichenberger, A. P.; Choutko, A.; Riniker, S.; Winger, M.; Mark, A. E.; van Gunsteren, W. F. *Eur. Biophys. J. Biophys. Lett.* **2011**, *40*, 843-856.
15. van Gunsteren, W. F.; Dolenc, J.; Mark, A. E. *Curr. Opin. Struct. Biol.* **2008**, *18*, 149-153.
16. Torda, A. E.; Brunne, R. M.; Huber, T.; Kessler, H.; van Gunsteren, W. F. *J. Biomol. NMR* **1993**, *3*, 55-66.
17. Kaptein, R.; Zuiderweg, E. R. P.; Scheek, R. M.; Boelens, R.; van Gunsteren, W. F. *J. Mol. Biol.* **1985**, *182*, 179-182.
18. Torda, A. E.; Scheek, R. M.; van Gunsteren, W. F. *Chem. Phys. Lett.* **1989**, *157*, 289-294.

19. Huber, T.; Torda, A. E.; van Gunsteren, W. F. *J. Comput.-Aided Mol. Des.* **1994**, *8*, 695-708.
20. Christen, M.; Keller, B.; van Gunsteren, W. F. *J. Biomol. NMR* **2007**, *39*, 265-273.
21. <http://www.gromos.net>
22. Berendsen, H. J. C.; Postma, J. P. M.; van Gunsteren, W. F.; Hermans, J., In: *Intermolecular forces*; B. Pullman (Ed.). Reidel, Dordrecht, The Netherlands, 1981, pp. 331-342.
23. Geerke, D. P.; Oostenbrink, C.; van der Vegt, N. F. A.; van Gunsteren, W. F. *J. Phys. Chem. B* **2004**, *108*, 1436-1445.
24. Walser, R.; Mark, A. E.; van Gunsteren, W. F.; Lauterbach, M.; Wipff, G. *J. Chem. Phys.* **2000**, *112*, 10450-10459.
25. Pardi, A.; Billeter, M.; Wuthrich, K. *J. Mol. Biol.* **1984**, *180*, 741-751.
26. Berendsen, H. J. C.; Postma, J. P. M.; van Gunsteren, W. F.; Dinola, A.; Haak, J. R. *J. Chem. Phys.* **1984**, *81*, 3684-3690.
27. Ryckaert, J. P.; Ciccotti, G.; Berendsen, H. J. C. *J. Comput. Phys.* **1977**, *23*, 327-341.
28. Tironi, I. G.; Sperb, R.; Smith, P. E.; van Gunsteren, W. F. *J. Chem. Phys.* **1995**, *102*, 5451-5459.
29. Daura, X.; van Gunsteren, W. F.; Mark, A. E. *Proteins-Struct. Funct. Genet.* **1999**, *34*, 269-280.
30. Dolenc, J.; Missimer, J. H.; Steinmetz, M. O.; van Gunsteren, W. F. *J. Biomol. NMR* **2010**, *47*, 221-235.